ELSEVIER

1359-8368(95)00002-X

Composites: Part B **27B** (1996) 11–23

1359-8368/96/$15.00

Concrete as a new strain/stress sensor

Pu-Woei Chen and D. D. L. Chung
Composite Materials Research Laboratory, State University of New York at Buffalo, Buffalo, NY 14260-4400, USA
(Received 20 September 1994; accepted 19 March 1995)

A new strain/stress sensor technology was developed, based on the concept of short electrically conducting fiber pull-out that accompanies slight and reversible crack opening. The fiber pull-out reversibly increases the composite's electrical resistance, which is the signal provided by the sensor under static or cyclic loading. The new technology was manifested in concrete and mortar containing electrically conducting short fibers (e.g. carbon fibers and steel fibers), but not in those containing no fibers or those containing non-conducting (polyethylene) fibers. Carbon fibers worked best. They served to greatly decrease the crack height, so that reversible pull-out of the crack bridging fibers occurred. Even in the elastic regime, a part of the resistance change was irreversible, such that it provided memory of the first deformation; this is due to permanent damage, probably associated with the increase in fiber/matrix contact electrical resistivity due to the interface bond weakening. The stress at which this damage began was much lower under tension than compression. The ratio of the contribution to the fractional resistance increase by the reversible part to that by the irreversible part was much higher under tension than compression. The irreversible part increased with increasing irreversible strain, which increased with increasing stress amplitude. The fractional increase in resistance at fracture was much larger under compression than under tension, was much larger for mortars than concretes at similar volume fractions, and was quite independent of the loading rate.

(Keywords: concrete; smart; sensor; strain; stress; carbon fibers)

INTRODUCTION

Strain/stress sensing is a function required of smart structures. The sensing of irreversible strain allows structural health monitoring. The sensing of reversible strain allows dynamic load monitoring. In general, the sensing of reversible strain is more challenging than that of irreversible strain, since reversible strain can only be monitored in real time whereas irreversible strain does not have to be monitored in real time. Furthermore, reversible strain tends to be smaller than irreversible strain.

The sensing function refers to the ability to provide an electrical (less commonly optical) response to a strain/stress stimulus. Requirements of the sensor include the following: (i) wide strain/stress range of detection (from small strains up to failure); (ii) response being reversible upon stimulus removal (necessary for repeated use of the sensor); (iii) ease of measuring the response (without the need of expensive peripheral equipment); (iv) presence of the sensor having no bad effect on the structural properties of the structure; (v) chemical stability and durability; and (vi) low cost (important for civil structures). Existing sensors include strain gages, optical fibers and piezoelectric sensors. All such sensors suffer from their high cost, poor durability and the need for expensive peripheral equipment, such as electronics and lasers. As a result, the use of sensors in civil structures is far from being common. In this work, a new sensor technology was developed. In this technology, concrete itself is the sensor. There is no need to embed strain gages, optical fibers or other sensors in the concrete, since the concrete itself is the sensor.

The development of the new sensor technology required the use of a concept that is different from any of those behind the existing sensor technologies. Previously known origins of reversible stress-induced electrical effects include: (i) change in electrical resistance of a metal wire or film upon straining; (ii) change in light throughput of optical fiber upon deformation; (iii) change in electrical dipole moment per unit volume upon straining (i.e. the piezoelectric effect); and (iv) change in separation between adjacent conducting filler units in a non-conducting matrix (i.e. piezoresistivity, applicable to ductile matrices such as polymers). The new sensor technology of this work made use of a new origin of the reversible stress-induced electrical effect. This new origin is the reversible change in fiber/matrix contact electrical resistivity upon straining a composite material containing electrically conducting short fibers and a

somewhat conducting (less conducting) matrix. The increase in fiber/matrix contact resistivity is due to slight pull-out of the crack bridging fiber. This contact resistivity increase causes an increase in the composite's electrical resistance, which is the response to the strain/stress stimulus. The use of fiber bridging[1] to control the crack opening so that it is small and reversible is the key to the ability of the material to serve as a sensor. Concrete is somewhat electrically conducting, so it satisfies a basic requirement for the matrix of a composite material that senses using the new concept.

The first report of the smart behavior of carbon fiber reinforced concrete was given by the authors in Ref. 2, which was limited to the smart behavior of mortars during compressive deformation. This paper extends the work from compression to tension and flexure and from mortars to concretes. Furthermore, this paper provides scientific elucidation of the smart behavior.

The ability to serve as a stress sensor means that a highway utilizing conducting fiber reinforced concrete has built-in pressure (weight) measurement capability throughout the highway for traffic monitoring in real time. The addition of conducting fibers to concrete not only decreases the volume resistivity of the concrete, but also decreases the contact resistivity between concrete and a metal[3]. This behavior is a consequence of the partial protrusion of the short fibers out of the concrete surface and enables the electrical probing of concrete with a metal probe to be very convenient. A good electrical contact can be achieved simply by touching the concrete with the metal probe. No conducting medium (such as silver paint) is needed between the concrete and the probe.

Associated with the decrease in the volume electrical resistivity due to the presence of the conducting fibers is the increase in the electromagnetic interference (EMI) shielding effectiveness of the concrete[4]. The shielding ability is valuable for structures housing electronics. Also associated with the decrease in resistivity is the increase in anti-static ability, which is useful for the floors of buildings housing electronics.

The addition of carbon fibers to concrete not only makes the concrete smart, it makes the concrete a better structural material. The improvement in the structural properties include increase in the flexural strength, flexural toughness[5–13] and freeze–thaw durability, and decrease in the drying shrinkage[5]. The decrease in drying shrinkage is valuable for the use of concrete for pothole repair, as the bonding between old concrete (already shrunk) and new concrete is much improved if the new concrete contains carbon fibers[14].

Effective use of carbon fibers in concrete requires dispersion of the short fibers, which are only 10 μm in diameter. The dispersion is greatly enhanced by the use of dispersants[15]. Examples of dispersants are methylcellulose[5], latex[6] and silica fume[5–13]. This paper reports on the effect of the dispersant on the smart performance as well as the structural properties of the concrete.

EXPERIMENTAL

Raw materials

Unless noted otherwise, the fibers used were carbon fibers. They were short, isotropic pitch based and unsized. The nominal fiber length was 5 mm. The fiber properties are shown in *Table 1*. Fibers in the amount of 0.5% by weight of cement were used, unless stated otherwise. The aggregate used was natural sand (100% passing 2.36 mm sieve, 99.91% SiO_2); the particle size analysis of which is shown in *Figure 1* of Ref. 15. *Table 2* describes the various raw materials used. *Table 3* describes the four types of mortar studies. They are: (i) plain mortar; (ii) plain mortar with latex; (iii) plain mortar with methylcellulose; and (iv) plain mortar with methylcellulose and silica fume. The latex, methylcellulose and silica fume were added to disperse the fibers, but in each category such additives were used whether fibers were present or not in order to obtain the effect of the fiber addition alone. In addition, latex and silica fume served to enhance the fiber/matrix bonding.

The water reducing agent powder used was TAMOL SN (Rohm and Haas) which contained 93–96% sodium salt of a condensed naphthalenesulfonic acid. In general, the slump of carbon fiber reinforced cement tends to decrease with increasing carbon fiber content. Therefore,

Table 1 Properties of carbon fibers

Filament diameter	10 μm
Tensile strength	690 MPa
Tensile modulus	48 GPa
Elongation at break	1.4%
Electrical resistivity	3.0×10^{-3} Ω.cm
Specific gravity	1.6 g cm^{-3}
Carbon content	98 wt %

Table 2 List of raw materials

Material	Source
Portland cement Type I	Lafarge Corporation (Southfield, MI)
TAMOL SN Sodium salt of a condensed naphthalenesulfonic acid (93–96%) Water (51–54%)	Rohm and Haas Company (Philadelphia, PA)
Methocel, A15-LV Methylcellulose	Dow Chemical Corporation (Midland, MI)
Colloids 1010 Defoamer	Colloids, Inc. (Marietta, GA)
Latex 460NA Styrene butadiene (40–60%) Water (40–60%) Stabilizer (1–5%)	Dow Chemical Corporation (Midland, MI)
Antifoam 2410 Polydimethylsiloxane (10%) Water, preservatives and emulsifiers (90%)	Dow Corning Corporation (Midland, MI)
Silica fume	Elkem Materials Inc. (Pittsburgh, PA)
Carboflex Carbon fibers	Ashland Petroleum Company (Ashland, KY)

we used various amounts of this water reducing agent in order to maintain the mortar at a reasonable flow value in the range of 150 ± 50 mm.

The latex was a styrene butadiene copolymer emulsion; it was used in the amount of 20% of the weight of the cement. The antifoam (Dow Corning 2410, an emulsion) used was in the amount of 0.5% of the weight of the latex; it was used whenever latex was used. Methylcellulose in the amount of 0.4% of the cement weight was used. The defoamer (Colloids 1010) used along with it was in the amount of 0.13 vol%; it was used whenever methylcellulose was used.

Mixing procedure

A Hobart mixer with a flat beater was used for mixing. For the case of mortar containing latex, the latex, antifoam and carbon fibers were mixed first by hand for about 1 min and then cement, sand, water and the water reducing agent were successively added and mixed in the Hobart mixer for 5 min. For the case of mortar containing methylcellulose, the defoamer and then the fibers were added to an aqueous methylcellulose solution and stirred by hand for about 2 min. Then this mixture, cement, sand, water and water reducing agent (and silica fume, if applicable) were mixed in the Hobart mixer for 5 min.

For the case of concrete, only one formulation was used, i.e. that involving methylcellulose and silica fume. The mixing procedure is quite similar to that for the corresponding mortar. Methylcellulose was dissolved in water; after that, the defoamer and then the fibers were added and stirred by hand for about 2 min. Then this mixture, cement, fine aggregate (Aggregate B described in Ref. 5), silica fume and then the water reducing agent were mixed in the Hobart mixer for 5 min. Subsequently the mix was poured into a stone concrete mixer to which the coarse aggregate (Aggregate D described in Ref. 5) was added and then mixing was conducted for about 3 min. After pouring the mix into oiled molds, a vibrator was used to decrease the amount of air bubbles.

Curing procedure

The specimens were demolded after 1 day and then allowed to cure at room temperature in air for 7 days. Unless stated otherwise, regular room humidity (about 10% RH) was used. In some cases, 60% RH was used.

Testing procedure

Resistance measurements were all made at a DC current in the range from 0.1 to 4 A. The specimen dimensions depended on the deformation code—compressive, tensile or flexural. They are all in accordance with ASTM standards for mortars and concretes. For all the tests, six specimens of each type were used.

For compressive testing according to ASTM C109-80, mortar specimens were prepared by using a 2 × 2 × 2 in (5.1 × 5.1 × 5.1 cm) mold. For compressive testing according to ASTM C39-83b, concrete specimens were

Table 3 Mix proportions and electrical resistivity of various types of mortar

Test	Sample	Fiber vol%	Water/ cement ratio	Sand/ cement ratio	Latex/ cement ratio	Meth*/ cement (%)	SF**/ cement ratio	WR+/ cement (%)	Electrical resistivity (Ω.cm)
Compressive	Plain mortar	0	0.45	1.5	0	0	0	0	1.46×10^5
	Plain mortar	0	0.3	1.0	0.2	0	0	0	2.71×10^5
	with latex	0.37	0.3	1.0	0.2	0	0	0	1.05×10^5
	Plain mortar	0	0.45	1.5	0	0.4	0	0	1.47×10^5
	with meth	0.24	0.45	1.5	0	0.4	0	2	8.33×10^4
	Plain mortar	0	0.45	1.5	0	0.4	0.15	2	2.09×10^5
	with meth and SF	0.24	0.45	1.5	0	0.4	0.15	2	3.19×10^3
Tensile	Plain mortar	0	0.3	0	0	0	0	0.5	1.50×10^5
	Plain mortar	0	0.23	0	0.2	0	0	0	2.75×10^5
	with latex	0.53	0.23	0	0.2	0	0	0	9.87×10^4
	Plain mortar	0	0.32	0	0	0.4	0	0.5	1.49×10^5
	with meth	0.53	0.32	0	0	0.4	0	1	2.53×10^4
	Plain mortar	0	0.35	0	0	0.4	0.15	3	2.32×10^5
	with meth and SF	0.53	0.35	0	0	0.4	0.15	3	2.14×10^3
Flexural	Plain mortar	0	0.475	1.0	0	0	0	0.5	1.46×10^5
	Plain mortar	0	0.23	1.0	0.2	0	0	0.5	2.71×10^5
	with latex	0.35	0.23	1.0	0.2	0	0	1.5	1.12×10^5
	Plain mortar	0	0.475	1.0	0	0.4	0	1	1.47×10^5
	with meth	0.35	0.475	1.0	0	0.4	0	1	5.73×10^4
	Plain mortar	0	0.475	1.0	0	0.4	0.15	2	2.09×10^5
	with meth and SF	0.35	0.475	1.0	0	0.4	0.15	2	2.80×10^3

* Meth = methylcellulose
** SF = silica fume
+ WR = water reducing agent

prepared using a 102 mm (4 inch) diameter × 203 mm (8 inch) length mold. Compression testing was performed using a hydraulic Material Testing System (MTS). The cross-head speed was 1.27 mm/min, unless noted otherwise.

Dog-bone shaped specimens of dimensions 80 × 60 × 20 mm in the narrowest part of the dog-bone shape were used for tensile testing. They were prepared by using molds of the same shape and size. Tensile testing was performed using a screw type mechanical testing system (Sintech 2/D). The loading speed was 1.27 mm/min, unless noted otherwise.

During compressive or tensile loading up to fracture, the strain was measured by the cross-head displacement in compressive testing or by a strain gage in tensile testing, while the fractional change in electrical resistance was measured using the four-probe method. The resistance was measured along the stress axis. The electrical contacts were made by silver paint applied along the whole perimeter in four parallel planes perpendicular to the stress axis. The inner two contacts were for voltage measurement, whilst the outer two contacts were for passing a current. Although the spacing between the contacts increased upon tensile deformation and decreased upon compressive deformation, the change was so small that the measured resistance remained essentially proportional to the volume resistivity. Testing was performed either in one cycle up to the breaking stress or in multiple cycles upon loading up to a fraction (1/3 under compression and ~1/2 under tension, unless stated otherwise) of the breaking stress (compressive/tensile).

Flexural testing was performed by three-point bending (ASTM C348-80), with a span of 140 mm (5.5 in). The specimen size was 40 × 40 × 160 mm. Flexural testing was performed using a screw type mechanical testing system (Sintech 2/D). The cross-head speed was 1.27 mm/min. During flexural loading up to fracture, the fractional change in electrical resistance was measured separately at the top surface (side under compression) and the bottom surface (side under tension). Electrical contacts were made by silver paint applied along four parallel lines (perpendicular to the long axis of the specimen) on each of the two opposite surfaces of the specimen.

RESULTS AND DISCUSSION

Table 4 summarizes the results of simultaneous compressive/tensile flexural testing and electrical resistivity measurement along the stress axis. The mechanical testing results include the ultimate strength and ductility. The electrical probing gave as raw result the resistance R between the two voltage probes in the four-probe set-up. *Table 4* gives the fractional change in R at the point of fracture, i.e. $\Delta R/R_o$, where R_o is the original resistance. The resistivity ρ is related to the resistance R by the equation

$$\rho = R\frac{A}{d}, \quad (1)$$

where A is the cross-sectional area and d is the distance between the voltage probes. For compressive testing, $d = 1$ and 4 cm for mortars and concretes, respectively; for tensile testing $d = 4$ cm (for mortars only); for flexural testing $d = 8$ cm (for mortars only). Since the dimensional changes are small during the deformation up to fracture, the fractional change in the electrical resistivity (i.e. $\Delta\rho/\rho_o$ where ρ_o is the original resistivity) is almost the same as $\Delta R/R_o$. For tensile and flexural testing, $\Delta R/R_o$ exactly equals $\Delta\rho/\rho_o$ because of the low ductility under tension or flexure. For compressive testing, $\Delta\rho/\rho_o$ is slightly larger than $\Delta R/R_o$. For example, $\Delta R/R_o$ values of 4.1, 10.42, and 21.14 correspond to $\Delta\rho/\rho_o$ values of 4.1, 10.44 and 21.18, respectively. The quantity $\Delta R/R_o$ is useful to field

Table 4 Results of simultaneous compressive/tensile/flexural testing and electrical resistivity measurement along the stress axis

	Compressive			Tensile			Flexural		
	Strength (MPa)	Ductility (%)	$\Delta R/R_o^+$	Strength (MPa)	Ductility (%)	$\Delta R/R_o^+$	Strength (MPa)	Ductility (%)	$\Delta R/R_o^{+*}$
Plain mortar	35.6	0.16	69.5	0.88	0.004	0.88	3.64	0.002	0.59/0.72
L	38.6	0.24	30	3.03	0.0352	0.6	5.99	0.003	0.21/0.70
L + 0.37 vol% F	37.8	0.17	4.1	—	—	—	—	—	—
L + 0.53 vol% F	—	—	—	3.15	0.0413	0.053	—	—	—
L + 0.35 vol% F	—	—	—	—	—	—	8.64	0.006	0.136/0.058
M	34.5	0.17	3.4	1.37	0.0209	0.18	3.43	0.005	1.76/0.55
M + 0.24 vol% F	33.6	0.15	10.42	—	—	—	—	—	—
M + 0.53 vol% F	—	—	—	1.95	0.0192	0.034	—	—	—
M + 0.35 vol% F	—	—	—	—	—	—	4.97	0.009	0.184/0.126
M + SF	42.7	0.16	9.7	0.83	0.088	0.037	3.94	0.002	0.67/0.32
M + SF + 0.24 vol% F	41.0	0.19	21.14	—	—	—	—	—	—
M + SF + 0.53 vol% F	—	—	—	1.88	0.0173	0.051	—	—	—
M + SF + 0.35 vol% F	—	—	—	—	—	—	5.11	0.004	0.121/0.104

* Under compression/under tension
+ At fracture
L = latex; M = methylcellulose; SF = silica fume; F = fibers

application of this *in-situ* health monitoring technique. The quantity $\Delta\rho/\rho_o$ is more meaningful scientifically.

In compressive, tensile and flexural cases, $\Delta R/R_o$ is positive, i.e. the resistivity increases as deformation takes place. This is because flaws are generated as deformation occurs. However, $\Delta R/R_o$ at fracture is much larger under compression than under tension or flexure. This is due to the much higher ductility under compression than under tension or flexure. In all cases where the mortar contains no fibers, $\Delta R/R_o$ varies randomly with strain/stress, though the amplitude of the variation is large and is larger under both compression and tension in the presence of latex than methylcellulose or methylcellulose + silica fume, as shown in *Table 4*. In other words, there was no correlation between $\Delta R/R_o$ and strain/stress. Thus, the smart behavior requires the presence of the fibers.

The magnitude of $\Delta R/R_o$ depends on the ingredients (other than the fibers) in the mortar. Under compression, the use of methylcellulose + silica fume gave the largest $\Delta R/R_o$, while the use of latex gave the smallest. Under tension, the use of latex gave the largest $\Delta R/R_o$, while the use of methylcellulose gave the smallest. Under flexure, the use of methylcellulose gave the largest $\Delta R/R_o$. These differences are partly due to the dependence of ρ_o on the type of ingredients present, as these ingredients help the dispersion of the fibers and are present at different concentrations (*Table 3*). At a given fiber volume fraction, latex yielded higher ρ_o than either methylcellulose or methylcellulose + silica fume, whether fibers were present or not. When fibers were absent, methylcellulose yielded the lowest ρ_o. When fibers were present, methylcellulose + silica fume yielded the lowest ρ_o; this is partly why methylcellulose + silica fume gave the highest $\Delta R/R_o$ under compression to fracture. Another reason is that methylcellulose + silica fume gave the highest compressive ductility when fibers were present. Since methylcellulose + silica fume gave higher ρ_o than methylcellulose (without silica fume) when fibers were absent, but lower ρ_o than methylcellulose when fibers were present, the silica fume appears to help the fiber dispersion, thereby making the fibers more effective in lowering the resistivity. Since smart performance was observed in all the fiber containing mortars and not observed in any of the mortars without fibers, the maximum ρ_o allowed for a smart mortar appears (falsely, as shown later) from *Table 3* to be between 1.12×10^5 and 1.46×10^5 Ω.cm. However, the small difference in resistivity between mortars without fibers and those with fibers suggests that the decrease in resistivity alone cannot explain why the carbon fibers were able to render the mortar smart. The effect of the fibers on the cracking plays an important role, as described later.

Simultaneous tensile testing and electrical resistivity measurement along the stress axis were conducted on mortars with fiber volume fractions 0.53, 1.06, 2.12, 3.18 and 4.24% (corresponding to fibers in amounts of 0.5, 1.0, 2.0, 3.0 and 4.0% of the cement weight). The results are shown in *Table 5*. The tensile strength increased with increasing fiber content up to 2.12% for the cases of mortars with latex or methylcellulose and 3.18% for the case of mortar with methylcellulose and silica fume. Above these fiber contents, the tensile strength decreased, due to the decreased workability and the resulting higher void content[15]. The value of $\Delta R/R_o$ did not vary much with the fiber content (*Table 5*), even though the value of ρ_o decreased significantly with increasing fiber content (*Table 5* and *Figure 1*). This means that a very low electrical resistivity is not required for the smart behavior to occur; a low value of ρ_o does not result in a large value of $\Delta R/R_o$.

Figures 2–4 give the plot of $\Delta R/R_o$ vs strain (or displacement in the case of flexural loading), together with the simultaneously obtained plot of stress vs strain (or displacement in the case of flexural loading), for compressive, tensile and flexural loading, respectively, for mortars containing methylcellulose and fibers. In the case of flexural loading, $\Delta R/R_o$ is given for the side of the specimen under compression as well as the side of the specimen under tension; $\Delta R/R_o$ is larger for the side under compression. *Figures 5* and *6* give the plots obtained under compression for plain mortar (without any dispersant or fiber). As shown by *Figure 6*, $\Delta R/R_o$ has no correlation with strain/stress when fibers are absent. *Figure 5* (which is *Figure 6* in a coarser vertical scale) shows that upon compressive fracture, $\Delta R/R_o$ abruptly increases in plain mortar, because of cracking. Thus, plain mortar can provide one-time (not repeated) failure sensing. In contrast, the addition of carbon fibers

Table 5 Results of simultaneous tensile testing and electrical resistivity measurement

Sample	Fiber/cement ratio	L			M			M + SF		
		$\Delta R/R_o^+$	ρ_o (Ω.cm)	Strength (MPa)	$\Delta R/R_o^+$	ρ_o (Ω.cm)	Strength (MPa)	$\Delta R/R_o^+$	ρ_o (Ω.cm)	Strength (MPa)
Plain mortar	0	0.88	1.50×10^5	0.88	0.88	1.50×10^5	0.88	0.88	1.50×10^5	0.88
(+L)/(+M)/(+M + SF)	0	0.6	2.75×10^5	3.03	0.18	1.49×10^5	1.37	0.037	2.32×10^5	0.83
+ 0.53 vol% F	0.5%	0.053	9.87×10^4	3.15	0.034	2.53×10^4	1.95	0.051	2.14×10^3	1.88
+ 1.06 vol% F	1.0%	0.057	119	3.16	0.027	26.1	2.61	0.048	13.9	2.03
+ 2.12 vol% F	2.0%	0.048	19.7	3.65	0.033	16.9	3.05	0.063	5.02	2.84
+ 3.18 vol% F	3.0%	0.061	12.2	3.32	0.041	7.82	2.97	0.057	3.88	3.01
+ 4.24 vol% F	4.0%	0.047	7.96	2.92	0.043	2.84	2.65	0.055	3.58	2.49

$^+$ At fracture
L = latex; M = methylcellulose; SF = silica fume; F = fibers

allows dynamic sensing, even at strains way before fracture. Another contrast is that the addition of carbon fibers causes $\Delta R/R_0$ to abruptly decrease (not increase) upon compressive fracture (*Figure 2*), probably because the highly conducting carbon fibers collapse together upon compressive fracture.

Because $\Delta R/R_0$ is much larger under compression than under tension, the curve of $\Delta R/R_0$ versus strain is less noisy under compression than under tension. Therefore, consideration of the shape of the curve of $\Delta R/R_0$ versus strain is more meaningful under compression than under tension. Comparison of such curves (*Figure 2* and others not shown) under compression for the three dispersants shows that the curve for the case of methylcellulose (*Figure 2*) is most linear. However, all three curves deviate from linearity in a concave upward fashion, i.e. $\Delta R/R_0$ is less than the value corresponding to exact linearity when the strain is small. This characteristic is attributed to the fiber bridging of cracks. The bridging makes the cracks not contribute much to $\Delta R/R_0$. The fraction of cracks experiencing fiber bridging increased with decreasing strain. The less linear is the curve of $\Delta R/R_0$ versus strain, the more significant is the fiber bridging. Comparison of *Figure 2* and the corresponding plot for the case of methylcellulose + silica fume suggests that fiber bridging is more significant in the case of methylcellulose + silica fume than in the case of methylcellulose (without silica fume). This suggestion is consistent with the higher degree of fiber dispersion in the former case[15]. As the degree of fiber dispersion is low in the case of latex[15], the abrupt $\Delta R/R_0$ increase at a strain of 1×10^{-3} in the curve of $\Delta R/R_0$ versus strain for the case of latex (not shown) is probably not due to fiber bridging, but rather is

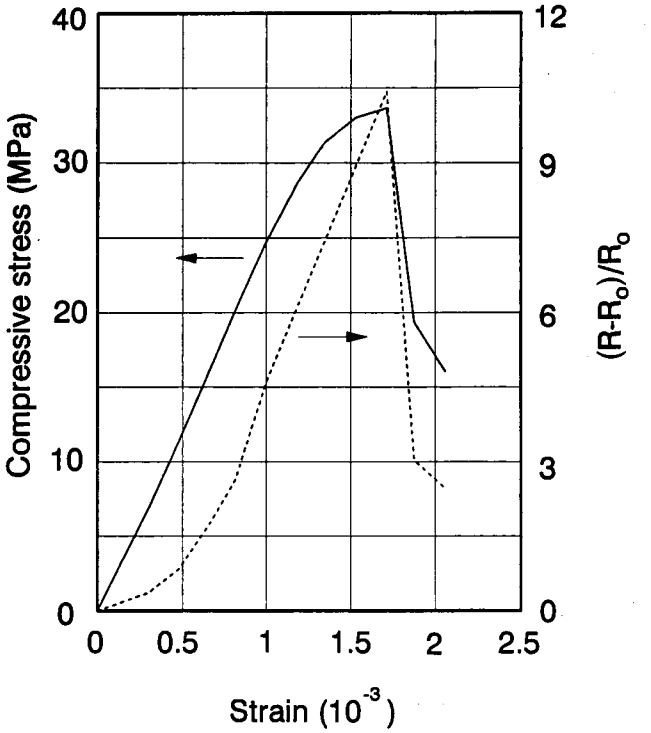

Figure 2 Plot of $\Delta R/R_0$ versus strain and plot of stress versus strain during static compressive testing for mortar containing methylcellulose and 0.24 vol% fibers

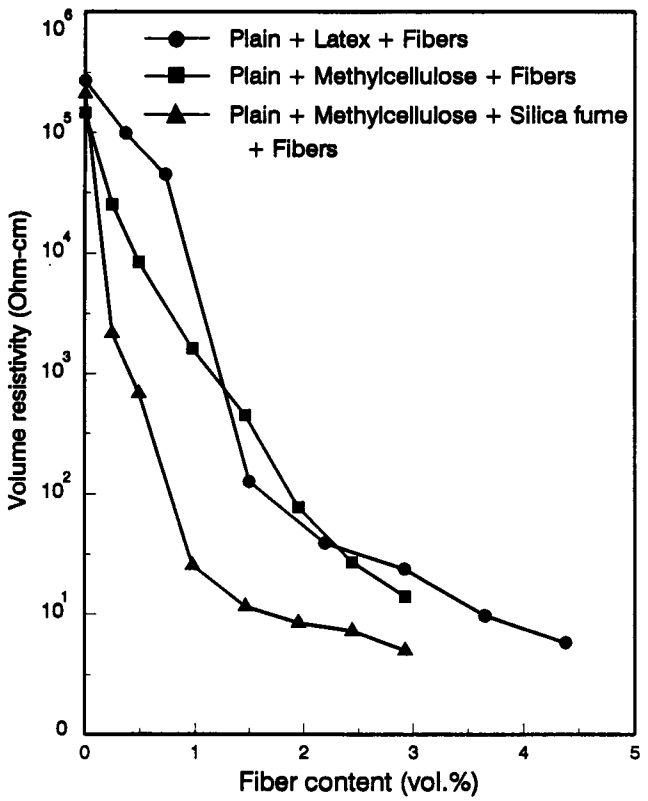

Figure 1 Volume electrical resistivity versus carbon fiber volume fraction for mortars containing: (a) latex; (b) methylcellulose; and (c) methylcellulose + silica fume

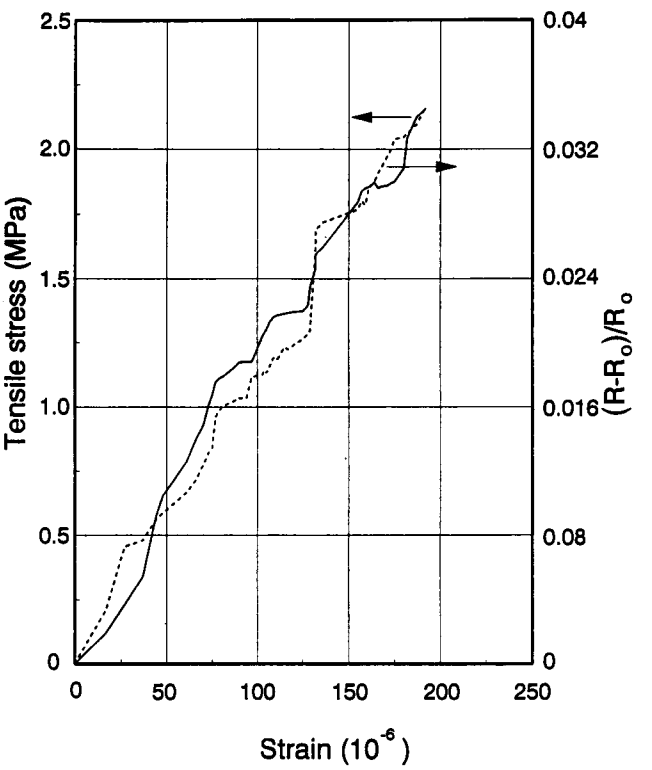

Figure 3 Plot of $\Delta R/R_0$ versus strain and plot of stress versus strain during static tensile testing for mortar containing methylcellulose and 0.53 vol% fibers

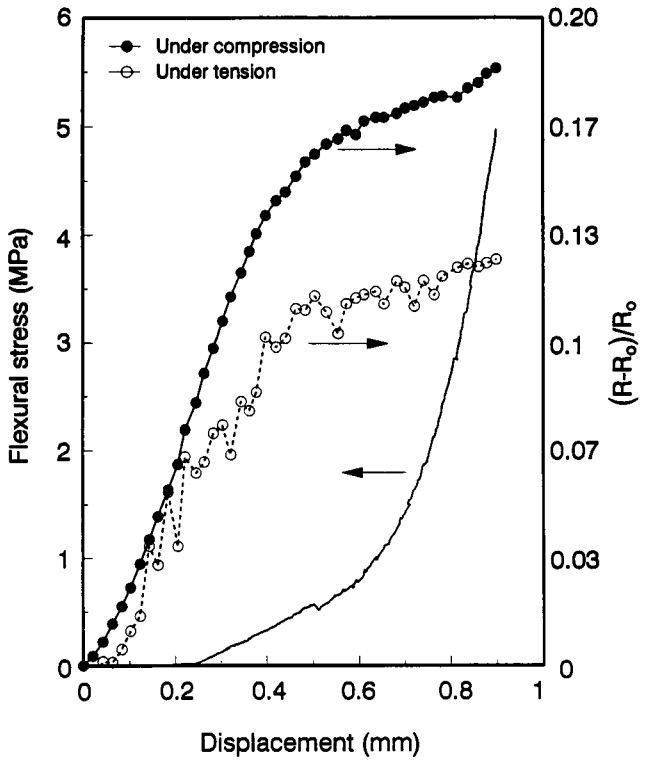

Figure 4 Plots of $\Delta R/R_o$ (at the compression side and tension side of the specimen) versus displacement and plot of stress versus displacement during static flexural testing for mortar containing methylcellulose and 0.35 vol% fibers

probably due to the plastic deformation tendency of latex. Plastic deformation does not require cracking, so the start of cracking occurs at a higher strain when plastic deformation (however slight) occurs.

The relationship between stress and $\Delta R/R_o$ (as shown in *Figures 2–4*) can be used as calibration curves that allow the mortars to be used as compressive/tensile stress sensors. Since $\Delta R/R_o$ is much larger under compression than under tension, the mortars are more effective as compressive stress sensors (pressure sensors) than tensile stress sensors. The linearity of such calibration curves is better for mortars containing methylcellulose than those containing methylcellulose + silica fume or containing latex.

Table 6 shows that the relative humidity during curing had negligible effect on $\Delta R/R_o$ at compressive/tensile fracture.

All the smart performance results given above were obtained during static loading. Consistent results were obtained under cyclic compressive/tensile loading, as described below. Without fibers, no smart behavior was observed at all. With fibers and methylcellulose, the smart behaviour was as shown in *Figures 7* and *8* for cyclic compressive and cyclic tensile loading, respectively. Under cyclic compressive loading within the regime where the strain was essentially fully reversible (*Figure 7*), the smart behavior was observed as: (i) irreversibly increasing $\Delta R/R_o$ during the first loading; (ii) reversibly increasing $\Delta R/R_o$ during unloading in any cycle; and (iii) reversibly decreasing $\Delta R/R_o$ during the second and subsequent loadings. The irreversibly

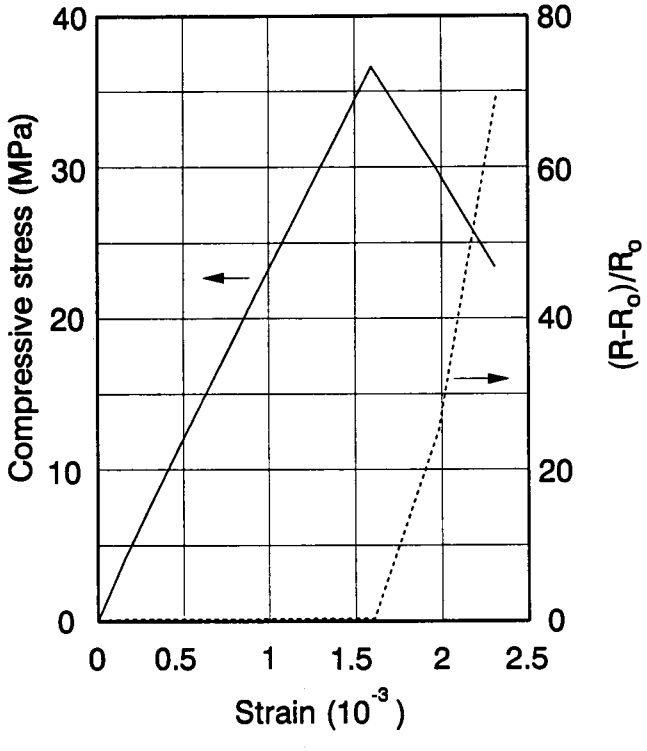

Figure 5 Plot of $\Delta R/R_o$ versus strain and plot of stress versus strain during static compressive testing for plain mortar

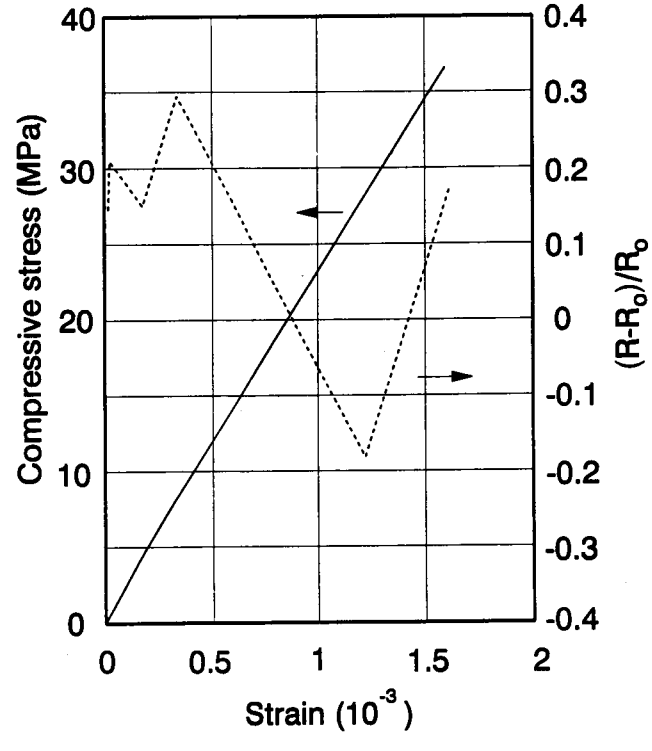

Figure 6 Plot of $\Delta R/R_o$ versus strain and plot of stress versus strain during static compressive testing for plain mortar. The zero of the scale for $\Delta R/R_o$ is half way up the graph, in contrast to *Figures 2–5*

increasing $\Delta R/R_0$ during the first loading (which involved no irreversible strain) is due to permanent damage, probably associated with the irreversible increase in the contact electrical resistivity at the fiber/matrix interface due to the weakening of that interface. Note that the increase in $\Delta R/R_0$ during first loading cannot be explained by the fibers becoming closer together, as increased proximity of adjacent fibers will decrease R rather than increase R. The irreversibly changed $\Delta R/R_0$ provides a memory indicating that prior loading has occurred. The reversibly increasing $\Delta R/R_0$ during unloading in any cycle is attributed to crack opening (i.e. increase in the length and/or height of a crack and the consequent fiber pull-out and increase in the fiber/matrix contact resistance), which was hindered under compressive loading. (The increase in the volume fraction of cracks contributes to the increasing $\Delta R/R_0$, but a simple calculation shows that the amount of cracks needed to provide the observed level of $\Delta R/R_0$ is too high, so that the crack volume alone is not sufficient to explain the observed $\Delta R/R_0$.) The reversibly decreasing $\Delta R/R_0$ during the second and subsequent loadings is attributed to the crack closure (i.e. decrease in the length or height of a crack and the consequent fiber push-in and decrease in fiber/matrix contact resistance) under compressive loading. The reversibility of the crack opening and closing is attributed to the fiber bridging across the crack, with fiber pull-out occuring during crack opening and fiber push-in occuring during crack closing. The occurrence of fiber pull-out requires a relatively weak fiber/matrix interface, which is provided by the interface weakening probably associated with the irreversible increase in $\Delta R/R_0$ prior to the fiber pull-out or crack opening. This means that permanent damage occurred early in the elastic deformation regime.

Under cyclic tensile loading within the regime where the strain was fully reversible (*Figure 8*), the smart behavior was observed as: (i) irreversibly increasing $\Delta R/R_0$ during the initial portion of the first loading; (ii) reversibly increasing $\Delta R/R_0$ during the latter portion of the first loading and during any subsequent loading; and (iii) reversibly decreasing $\Delta R/R_0$ during unloading in

Table 6 $\Delta R/R_0$ at compressive/tensile fracture at different values of the relative humidity

Relative humidity during curing	Compressive*	Tensile+
10%	4.1	0.053
60%	4.7	0.061

* Mortar containing latex and 0.37 vol% fibers
+ Mortar containing latex and 0.53 vol% fibers

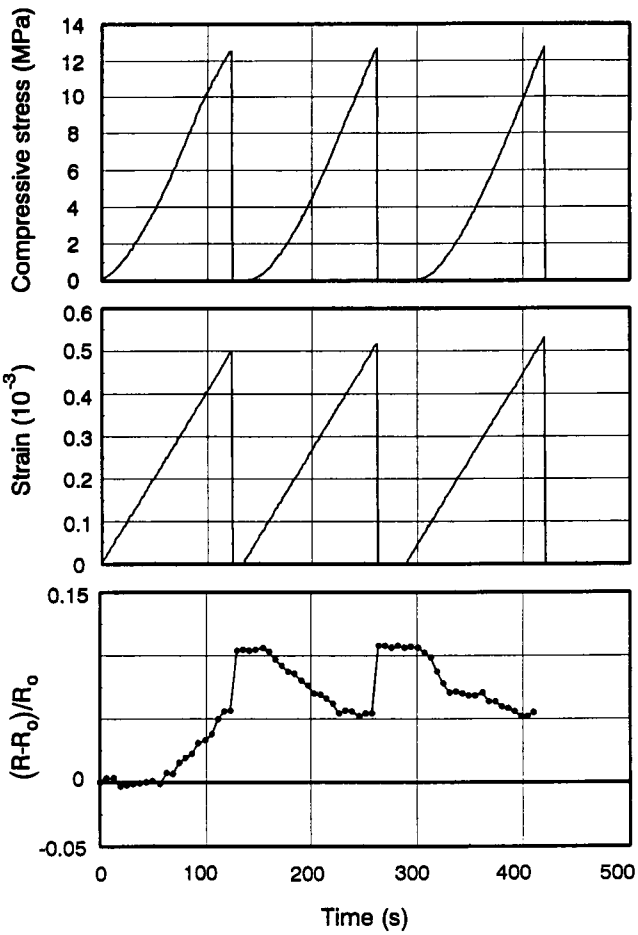

Figure 7 Plots versus time of $\Delta R/R_0$, compressive strain and compressive stress obtained during cyclic compressive testing for mortar containing methylcellulose and 0.24 vol% fibers

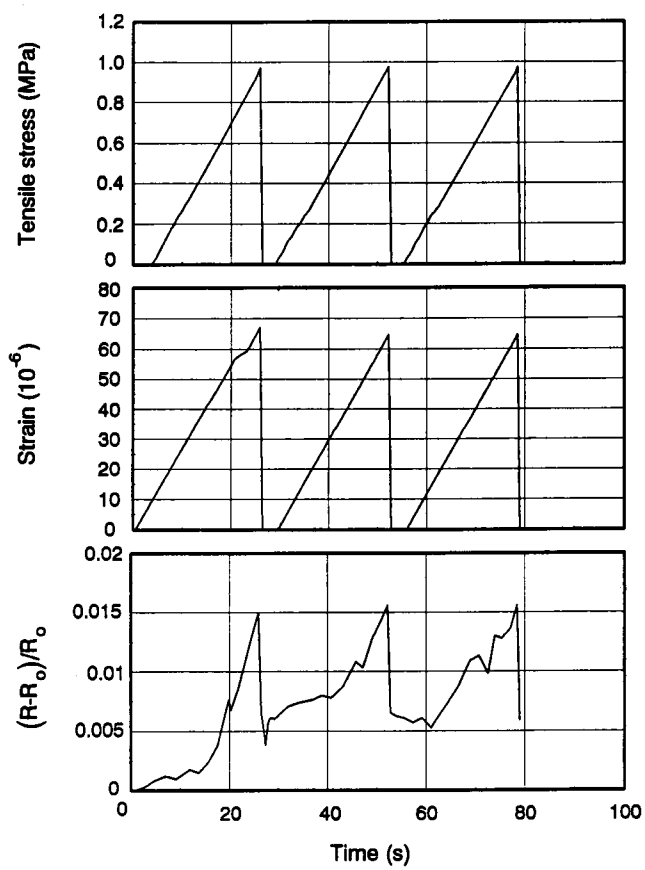

Figure 8 Plots versus time of $\Delta R/R_0$, tensile strain and tensile stress obtained during cyclic tensile testing for mortar containing methylcellulose and 0.53 vol% fibers

any cycle. The increase in $\Delta R/R_o$ during loading is attributed to crack opening, whereas the decrease in $\Delta R/R_o$ during unloading is attributed to crack closure. That the initial portion of the first loading exhibited irreversibly increasing $\Delta R/R_o$ whereas the latter portion was reversible is because the irreversible part is due to permanent damage, probably associated with fiber/matrix interface weakening, whereas the reversible part is due to fiber pull-out that accompanies crack opening. The stress at which the irreversible $\Delta R/R_o$ increase ends and the reversible $\Delta R/R_o$ increase starts is the stress at which the fiber/matrix interface is sufficiently weak for it to not restrain crack opening or fiber pull-out. The cracks under tension were preferentially oriented perpendicular to the stress axis. Similar results were obtained for mortars containing fibers, methylcellulose and silica fume and for mortars containing fibers and latex.

Under both cyclic compression and cyclic tension, the stress/strain at which the irreversible $\Delta R/R_o$ increase starts to occur is the stress/strain at which permanent damage, probably associated with the fiber/matrix interface weakening, starts to occur. *Table 7* lists these stress/strain values under compression and tension for the three formulations of carbon fiber reinforced mortars. The stress and strain values under both compression and tension are lower for the case of latex than in the case of methylcellulose or the case of methylcellulose + silica fume. This means that the fibre/matrix bonding is weaker in the case of latex. For all formulations, the stress for the interface to start to weaken was much lower under tension than compression. This is expected since tension acts in a direction to open up that interface, whereas compression acts to squeeze the interface.

Under cyclic tension, the stress/strain at which the reversible $\Delta R/R_o$ increase starts to occur is the stress/strain at which fiber pull-out (crack opening) starts. The value of the strain is 48×10^{-6}, 50×10^{-6} and 6.8×10^{-6} for (i) the mortar with latex and 0.53 vol% fibers, (ii) the mortar with methylcellulose and 0.53 vol% fibers, and (iii) the mortar with methylcellulose, silica fume and 0.53 vol% fibers, respectively. These strain values ($\sim 10^{-5}$) are much smaller than the values ($\sim 10^{-4}$) at which the tensile stress/strain curves (e.g. *Figure 3*) start to deviate from linearity. Irreversible damage (probably associated with the weakening of the fiber/matrix bonding) occurs before the occurrence of first crack opening (reversible), which in turn occurs much before the point at which the stress/strain curve starts to deviate from linearity.

All the data given above were obtained on mortars. Consistent results were obtained on concretes, as described below. Without fibers, no smart action was observed. The $\Delta R/R_o$ values are much lower for concretes than mortars at similar fiber volume fractions. *Table 8* lists the values of $\Delta R/R_o$ (at compressive fracture) and ρ_o for mortars and concretes containing 0.2 vol% fibers. At the same fiber volume fraction, ρ_o is much higher for concrete than mortar. In spite of the high ρ_o for carbon fiber reinforced concretes (even higher than those of plain mortars exhibiting no smart behavior, *Table 3*), the smart behaviour occurred, indicating that the occurrence of smart behavior is not governed by ρ_o. An increase in the carbon fiber volume fraction in the concrete decreased ρ_o and increased $\Delta R/R_o$, as shown in *Table 9*, but the increased $\Delta R/R_o$ is still much lower than the values for mortars, even when ρ_o of the concrete is below those of the mortars of *Table 3*. This means that the low $\Delta R/R_o$ of concretes is not due to the high ρ_o, but rather is due to the presence of the coarse aggregate, which makes the cracking control ability of the fibers less prominent. In spite of the low values of $\Delta R/R_o$ for concretes, the measurement of $\Delta R/R_o$ was not difficult, even at the lowest fiber content of 0.19 vol%.

Table 10 shows the reversible and irreversible parts of $\Delta R/R_o$ at the same fraction (1/3 under compression and $\sim 1/2$ under tension) of the fracture stress relative to $\Delta R/R_o$ at fracture for mortars with different dispersants. The fraction $(\Delta R/R_o)_{reversible}/(\Delta R/R_o)_{fracture}$ is much larger than the fraction $(\Delta R/R_o)_{irreversible}/(\Delta R/R_o)_{fracture}$ under compression for mortars when latex was the dispersant but the two fractions are equal when either methylcellulose or methylcellulose + silica fume was used

Table 7 Stress and strain at which the irreversible increase in $\Delta R/R_o$ starts to occur

	Stress (MPa)	Strain
Compression		
L + 0.37 vol% F	0.03	1.6×10^{-5}
M + 0.24 vol% F	0.35	2.5×10^{-5}
M + SF + 0.24 vol% F	0.29	9.7×10^{-5}
Tension		
L + 0.53 vol% F	0.001	2×10^{-8}
M + 0.53 vol% F	0.004	5.7×10^{-7}
M + SF + 0.53 vol% F	0.063	2.9×10^{-7}

L = latex; M = methylcellulose; SF = silica fume; F = fibers

Table 8 $\Delta R/R_o$ at compressive fracture and ρ_o for mortars and concretes containing 0.2 vol% carbon fibers

	$\Delta R/R_o$		$\rho_o(\Omega.cm)$	
Dispersant	Mortar*	Concrete+	Mortar*	Concrete+
Methylcellulose	10.42	0.37	8.33×10^4	3.70×10^6
Methylcellulose + silica fume	21.14	0.105	3.19×10^3	2.32×10^6

* 0.24 vol% carbon fibers
+ 0.19 vol% carbon fibers

Table 9 $\Delta R/R_o$ at compressive fracture, ρ_o and compressive strength for concretes with various carbon fiber volume fractions

Fiber volume fraction (%)	Fiber/cement ratio	$\Delta R/R_o$		ρ_o(Ω.cm)		Compressive strength (MPa)	
		M	M + SF	M	M + SF	M	M + SF
0.19	0.5%	0.37	0.103	3.70×10^6	2.32×10^6	23.39 (±9%)	26.90 (±8%)
0.38	1.0%	0.52	0.86	1.51×10^5	9.92×10^3	18.41 (±6%)	23.52 (±7%)
0.76	2.0%	1.01	1.37	1.26×10^3	1.69×10^3	12.64 (±7%)	18.84 (±9%)
1.14	3.0%	1.32	1.42	2.27×10^2	2.44×10^2	10.61 (±8%)	12.30 (±7%)

M = methylcellulose; SF = silica fume

Table 10 Reversible and irreversible parts of $\Delta R/R_o$ relative to $\Delta R/R_o$ at fracture for mortars under compression and tension

	$(\Delta R/R_o)/(\Delta R/R_o)_{fracture}$		
	L	M	M + SF
Compression			
Reversible	0.0034 (±15%)	0.0048 (±8%)	0.0047 (±9%)
Irreversible	0.0015 (±9%)	0.0048 (±8%)	0.0047 (±10%)
Tension			
Reversible	0.21 (±8%)	0.29 (±12%)	0.49 (±10%)
Irreversible	0.075 (±11%)	0.15 (±7%)	0.059 (±15%)

L = latex; M = methylcellulose; SF = silica fume

Table 11 Reversible and irreversible parts of $\Delta R/R_o$ relative to $\Delta R/R_o$ at fracture for mortars and concretes under compression

	$(\Delta R/R_o)/(\Delta R/R_o)_{fracture}$	
	M	M + SF
Mortars		
Reversible	0.0048 (±8%)	0.0047 (±9%)
Irreversible	0.0048 (±8%)	0.0047 (±10%)
Concretes		
Reversible	0.11 (±12%)	0.43 (±8%)
Irreversible	0.11 (±15%)	0.24 (±11%)

M = methylcellulose; SF = silica fume

as the dispersant. This is attributed to the plastic deformation tendency of latex, which facilitates crack opening and closing, thereby enhancing $(\Delta R/R_o)_{reversible}$ more than $(\Delta R/R_o)_{irreversible}$. Under tension, the fraction $(\Delta R/R_o)_{reversible}/(\Delta R/R_o)_{fracture}$ is much larger than the fraction $(\Delta R/R_o)_{irreversible}/(\Delta R/R_o)_{fracture}$ for all three dispersant cases. This characteristic under tension is attributed to the more important role of small cracks in affecting fracture in tension than in compression and the fact that cracks that can undergo reversible opening and closing are necessarily small. The fraction $(\Delta R/R_o)_{reversible}/(\Delta R/R_o)_{fracture}$ under tension is higher for the case of methylcellulose + silica fume than the case of methylcellulose or that of latex, because the degree of fiber dispersion is highest in the case of methylcellulose + silica fume[14], and that the fibers are responsible for controlling the crack opening so that reversible crack opening and closing is possible.

Table 11 shows the fractions $(\Delta R/R_o)_{reversible}/(\Delta R/R_o)_{fracture}$ and $(\Delta R/R_o)_{irreversible}/(\Delta R/R_o)_{fracture}$ under compression for mortars and concretes with the same dispersants. Both fractions are much higher for concretes than mortars. This means that crack development occurs earlier (at a lower stress relative to the fracture stress) during deformation in concretes than in mortars, probably because of the decreased effectiveness of the fibers in hindering crack opening when the coarse aggregate is present. That $(\Delta R/R_o)_{reversible}$ dominates $(\Delta R/R_o)_{irreversible}$ in concrete with methylcellulose + silica fume, but not in concrete with methylcellulose (and no silica fume) is attributed to the higher degree of fiber dispersion in the former case[15] and that the fibers are responsible for controlling the crack opening.

The fractions $(\Delta R/R_o)_{reversible}/(\Delta R/R_o)_{fracture}$ and $(\Delta R/R_o)_{irreversible}/(\Delta R/R_o)_{fracture}$ vary with the stress amplitude in cyclic loading, as shown in *Table 12*, where the stress amplitude is expressed as the maximum stress divided by the fracture stress. The fractions listed are for compression of mortars containing latex and 0.37 vol % carbon fibers. They increase with increasing stress amplitude, such that they are much larger when the stress amplitude is 0.50 than when the stress amplitude is 0.33 or below. This is attributed to the abrupt increase in crack concentration or size when the stress is increased from 0.33 to 0.50 of the fracture stress. The fraction $(\Delta R/R_o)_{reversible}/(\Delta R/R_o)_{fracture}$ increases most abruptly as the stress amplitude is increased from 0.40 to 0.50, whereas the fraction $(\Delta R/R_o)_{irreversible}/(\Delta R/R_o)_{fracture}$ increases most abruptly as the stress amplitude is increased from 0.33 to 0.40. The ratio of the reversible part of $\Delta R/R_o$ to the irreversible part of $\Delta R/R_o$ is smaller at a stress amplitude of 0.40 or above compared to those at lower stress amplitudes, because the abrupt increase in crack concentration or size when the stress is increased from 0.33 to 0.40 of the fracture stress is due mainly to irreversible crack opening rather than reversible crack opening. The ratio of the reversible part of $\Delta R/R_o$ to the irreversible part of $\Delta R/R_o$ is largest at a stress amplitude of 0.33 and decreases slightly with decreasing stress amplitude below 0.33, probably because there is a minimum amount of irreversible crack opening that is present at all stress amplitudes, so that the reversible part decreases slightly in relative importance when the stress amplitude is decreased below 0.33. At a stress amplitude of 0.40 or above, the ratio of the reversible part of $\Delta R/R_o$ to the irreversible part of $\Delta R/R_o$ is much smaller than that at a stress amplitude below 0.40. This is due to the abrupt increase of the irreversible strain when the stress amplitude is

Table 12 Effect of stress amplitude in cyclic compressive loading on the reversible and irreversible parts of $(\Delta R/R_o)/(\Delta R/R_o)_{fracture}$ and the reversible and irreversible parts of strain/$strain_{fracture}$ for mortar containing latex and 0.37 vol% carbon fibers

	$(\Delta R/R_o)/(\Delta R/R_o)_{fracture}$			Strain/$Strain_{fracture}$		
Maximum stress/ Fracture stress	Reversible	Irreversible	Reversible/ Irreversible	Reversible	Irreversible	Reversible/ Irreversible
0.75	0.039	0.244	0.16	0.29	0.44	0.66
0.65	0.037	0.102	0.36	0.29	0.33	0.88
0.50	0.032	0.115	0.28	0.38	0.12	3.17
0.40	0.0073	0.068	0.11	0.33	0.09	3.70
0.33	0.0034	0.0015	2.27	0.32	0.01	52.5
0.25	0.0025	0.0013	1.92	0.29	0.00	∞
0.20	0.0027	0.0017	1.59	0.27	0.00	∞

increased from 0.33 to 0.40. As shown in *Table 12*, the irreversible strain is zero at stress amplitudes of 0.20 and 0.25, is essentially zero at a stress amplitude of 0.33, abruptly increases when the stress amplitude is increased from 0.33 to 0.40, and increases monotonically with increasing stress amplitude from 0.40 to 0.75. On the other hand, the reversible strain does not vary much with the stress amplitude. *Table 12* shows good correlation between the irreversible strain and the irreversible part of $\Delta R/R_o$.

The combination of *Tables 10* and *12* shows that, at the same stress amplitude of 1/2 and for the same dispersant (latex), the ratio of the reversible contribution to $\Delta R/R_o$ to the irreversible contribution to $\Delta R/R_o$ is much higher under tension than under compression. This is again attributed to the more important role of small cracks in affecting fracture in tension than in compression and the fact that cracks that can undergo reversible opening and closing are necessarily small. The loading rate had negligible effect on the smart response, as shown by measuring $\Delta R/R_o$ under compression at loading rates of 0.64, 1.27 and 2.54 mm/min.

Table 4 also shows significant effects of the carbon fiber addition on the mechanical properties, especially the tensile and flexural properties. The values of the tensile strength for mortars with various carbon fiber volume fractions are shown in *Table 5*. The effectiveness of the fiber addition in improving the mechanical properties depends on the ingredients (other than the fibers) in the mortar. The use of latex gave the highest tensile and flexural strengths, while the use of methylcellulose + silica fume gave the highest compressive strength. The compressive strength decreased with increasing fiber volume fraction (*Table 9*). For the sake of a high compressive strength and low cost, the lowest fiber content corresponding to a fiber/cement ratio of 0.5% is recommended for both mortars and concretes used as sensors.

Similar effects of the carbon fiber addition on the flexural and compressive properties were observed for concretes as well as mortars. The effects in the case of concrete are described in *Table 9* and Ref. 5.

In order to investigate the origin of the smart behavior rendered by the carbon fiber addition, the effect of the fiber addition on the fracture pattern was microscopically examined. Optical microscope photographs (*Figure 9*) were obtained of the vertical edge surface of mortar cubes that had been compressed vertically on the horizontal surfaces up to about 70% of the fracture stress for (a) the mortar containing latex but no fibers, and (b) the mortar containing latex and 0.37 vol % fibers. As shown in *Table 4*, these two mortars have similar compressive strengths. The cracks are much narrower in

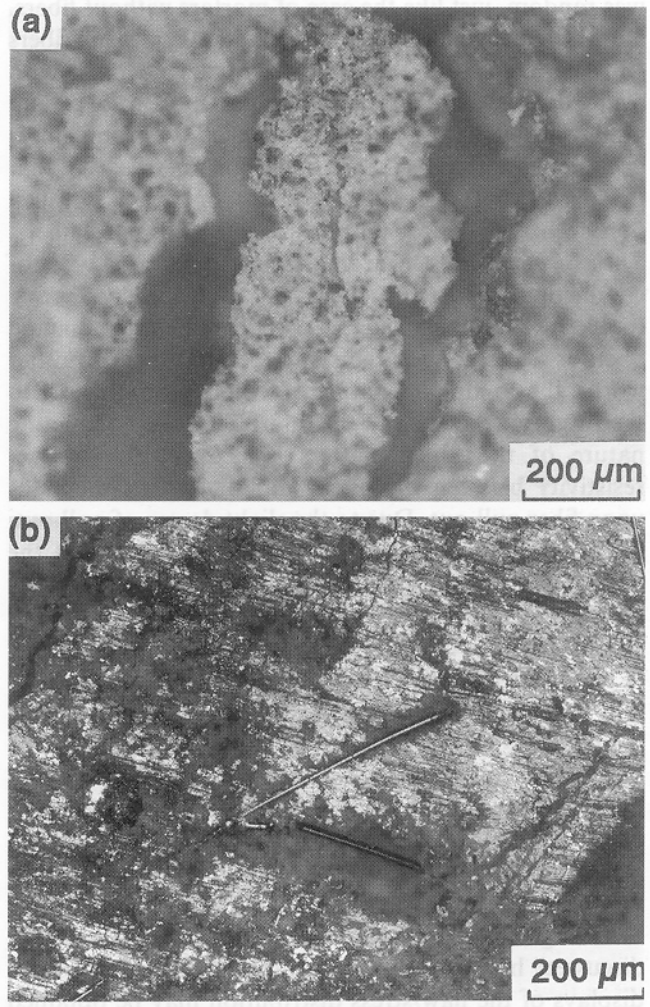

Figure 9 Optical micrographs of the cracks after compression to 70% of the fracture stress of (a) mortar containing latex but no fibers and (b) mortar containing latex and 0.37 vol% fibers. The straight features near the middle of (b) are fibers. A crack in (b) is the nearly vertical crooked line at the top center of the photograph

(b) than in (a) (100 μm in (a), <1 μm in (b)), indicating that the fibers cause crack opening control, which in turn results in the smart behavior. This means that the reversible fiber pull-out involves only slight fiber pull-out (<1 μm). Optical photographs were also obtained of the fracture paths of mortars in the form of test specimens that had been fractured under flexure. The fracture path was found to be quite straight in the plain mortar, but was increasingly tortuous and branched as the fiber volume fraction increased. The effect of the fibers on the crack height and crack tortuosity is consistent with the increased toughness[5] due to the fiber addition. Thus, the role of the fibers is not just to increase the conductivity of the concrete, but is to decrease the crack height and increase the crack tortuosity. This effect of the fibers on the fracture characteristics is responsible for the smart action.

Measurement of $\Delta R/R_o$ during static compression was also conducted on mortars containing polyethylene fibers (Allied-Signal, Inc., Spectra 900, diameter 38 μm, length 5 mm, density 0.97 g/cm^3, in the amount of 0.35 vol%, and used without any dispersant) instead of carbon fibers. The variation of $\Delta R/R_o$ with strain/stress was random, just like the case of mortars without fibers. On the other hand, the use of stainless steel fibers (International Steel Wool Co., diameter 60 μm, length 5 mm, density 7.8 g/cm^3, in the amount of 0.35 vol%, and used without any dispersant) instead of carbon fibers gave similar effects as the use of carbon fibers, except that the curve of $\Delta R/R_o$ versus stress or strain is much noisier, because of the poor dispersion of the steel fibers. These observations regarding the use of various types of conducting (carbon and steel) and non-conducting (polyethylene) fibers suggest that the use of conducting fibers is necessary for the smart performance. In other words, the conducting nature of the fibers contributes to the origin of the smart behaviour. That the conducting nature of the fibers matters is because the contact resistivity between the fibers and the matrix increases upon fiber pull-out. Due to the slight degree of pull-out, the change in contact area between the fibers and the matrix is negligible. Hence, the observed reversible increase in $\Delta R/R_o$ is not simply due to the high resistance of the cracks, but is largely due to the increase in fiber/matrix contact resistivity that accompanies fiber pull-out, which in turn accompanies crack opening. This interpretation is consistent with the fact that for each type of carbon fiber reinforced mortar (different types having different dispersants), the value of the reversible part of $\Delta R/R_o$ is smaller than the fractional increase in resistivity if the carbon fibers were all removed from that mortar, i.e. $(\rho_{\text{without fibers}} - \rho_{\text{with fibers}})/\rho_{\text{with fibers}}$.

In engineering implementation of the smart materials discussed here, two-dimensional or three-dimensional displays of the flaw/stress distribution may be obtained by electrical resistivity tomography. The new sensor technology reported here for concrete may be extended to other brittle composite materials, such as ceramic/matrix composites. Although this work used mainly carbon fibers to control crack opening, it may be possible to achieve the smart action with less conducting fibers, such as silicon carbide whiskers.

CONCLUSION

Mortars containing 0.2–4.2% by volume of short carbon fibers and concretes containing 0.2–1.1% by volume of the fibers were found to be capable of providing non-destructive *in-situ* structural health monitoring and stress sensing via electrical probing. Without the fibers, or with polyethylene fibers instead of carbon fibers, no smart behavior was observed. Fractional increases in the electrical resistivity along the stress axis by up to 21 (i.e. 2100%) during compressive loading to failure, up to 0.053 (i.e. 5.3%) during tensile loading to failure, and up to 0.184 (i.e. 18.4%) during flexural loading to failure were observed in the mortars. The weaker effect during tension or flexure was due to the much lower ductility under tension than compression. The effects were similar for different relative humidities during curing. Besides providing the smart performance, fiber addition at a fiber/cement ratio of only 0.5% increased the tensile and flexural strength, without affecting the compressive properties much. The smart behavior is attributed to the decrease in crack height. This results from the fiber addition and the consequent reversibility of bridging fiber pull-out during reversible crack opening. The sensing action manifests itself as an increase in the electrical resistance upon fiber pull-out. The resistance increase is attributed to the increase in fiber/matrix contact electrical resistivity upon fiber pull-out.

Both the smart performance and mechanical properties varied with the ingredients added for dispersing the fibers. Latex gave the highest tensile and flexural strengths and tensile ductility, the weakest smart performance under compression, the strongest smart performance under tension, and the most expensive mix. Methylcellulose + silica fume gave the lowest tensile strength and tensile ductility, the highest compressive strength and compressive ductility, and the strongest smart performance under compression. Methylcellulose (without silica fume) gave the lowest compressive strength and compressive ductility, the weakest smart performance under tension, and the strongest smart performance under flexure. The linearity between the fractional change in resistance ($\Delta R/R_o$) and strain/stress is best for methylcellulose.

Smart behavior was observed under cyclic compressive/tensile loading due to crack opening and closure. The electrical response ($\Delta R/R_o$) was reversible except for the first loading, which was 'remembered' by the smart material. The irreversible part of $\Delta R/R_o$ in the absence of irreversible strain is attributed to permanent damage, probably associated with fiber/matrix interface weakening, whereas the reversible part is attributed to crack opening (fiber pull-out) and crack closing (fiber push-in). The stress at which the irreversible part starts to

be non-zero is the stress at which the permanent damage mentioned above starts to occur; this stress is lower for latex than for methylcellulose or methylcellulose + silica fume as the dispersant, and is lower under tension than under compression. In case of some irreversible strain, the irreversible part is partly due to irreversible crack opening (or crack opening without control by a bridging fiber). The ratio of the contribution to $\Delta R/R_o$ by the reversible part to that by the irreversible part depends on the dispersant, the stress amplitude and the deformation mode (compression or tension). This ratio is higher for latex than for either methylcellulose or for methylcellulose + silica fume when the mortar is under compression. It drops abruptly (while the irreversible strain increases abruptly) when the stress amplitude under compression is increased from 0.33 to 0.40, at least for the case of latex as the dispersant. It is much higher under tension than under compression for the same dispersant and the same stress amplitude. Both fractions $(\Delta R/R_o)_{reversible}/(\Delta R/R_o)_{fracture}$ and $(\Delta R/R_o)_{irreversible}/(\Delta R/R_o)_{fracture}$ are higher under tension than compression and are higher for concretes than mortars.

Smart behavior was observed in concretes as well as mortars, though $\Delta R/R_o$ was much larger for mortars than concretes, because the fibers are less effective in controlling crack opening when a coarse aggregate is present. The value of $\Delta R/R_o$ was similar for mortars with various fiber volume fractions (0.2–4.2%), but increased slightly with increasing fiber volume fraction (0.2–1.1%) for concretes; this is due to the lower resistivity (ρ_o) of concretes compared to mortars at similar fiber volume fractions. The value of $\Delta R/R_o$ was quite independent of the loading rate.

REFERENCES

1 Li, V.C. *ASCE J. Materials in Civil Engineering* 1992, **4** (1), 41
2 Chen, P.-W. and Chung, D.D.L. *Smart Mater. Struc.* 1993, **2**, 22
3 Chen, P.-W. and Chung, D.D.L. *Smart Mater. Struc.* 1993, **2**, 181
4 Chiou, J.-M., Zheng, Q. and Chung D.D.L. *Composites* 1989, **20** (4), 379
5 Chen, P.-W. and Chung, D.D.L. *Composites* 1993, **24** (1) 33
6 Yang, X. and Chung, D.D.L. *Composites* 1992, **23** (6), 453
7 Furukawa, S., Tsuju, Y. and Otani, S. in *'Proc. 30th Japan. Congr. of Material Res.'*, 1986, p. 149
8 Akihama, S., Suenaga, T. and Banno, T. *Int. J. Cement Composites Lightweight Concrete* 1986, **8**, 21
9 Akihama, S., Kobayashi, M., Suenaga, T., Nakagawa, H. and Suzuki, K. Mechanical properties of carbon reinforced cement composite and the application to buildings (Part 2). Kajima Institute of Construction Technology Report 65, 1986
10 Ohama, Y., Sato, Y. and Endo, M. *'Proc. Asia-Pacific Concrete Technol. Conf. '86'*, 1986, p. 5.1
11 Park, S.B. and Lee, B.I. in *'Proc. 1990 Fall Mater. Res. Soc. Symp.'*, 1991, **211**, 247
12 Zheng, Q. and Chung, D.D.L. *Concr. Cem. Res.* 1989, **19**, 25
13 Larson, B.K., Drzal, L.J. and Sorousian, P. *Composites* 1990, **21**, 205
14 Chen, P.-W., Fu, X. and Chung, D.D.L. *Cem. Concr. Res.* 1995, **25**, 491
15 Chen, P.-W. and Chung, D.D.L. *Composites* (in press)